FE ANALYSIS OF STRAIN LOCALIZATION IN CONCRETE IN ELASTO-PLASTICITY AND DAMAGE MECHANICS WITH NON-LOCAL SOFTENING

JERZY BOBIŃSKI

Gdansk University of Technology,
Faculty of Civil and Environmental Engineering,
80-952 Gdansk, Narutowicza 11/12, Poland
bobin@pg.gda.pl

Abstract: Results of Finite Element Method (FEM) simulations of a strain localization in concrete specimens are presented. Two different continuum approaches have been used to model to behaviour of concrete: (i) an elasto-plastic constitutive law with the Drucker-Prager criterion in the compression regime and the Rankine criterion in the tensile regime, with isotropic hardening and softening and (ii) an isotropic continuum damage model with the equivalent strain corresponding to the Rankine failure criterion and modified Huber-Mises criterion in terms of strains, with exponential softening. Both constitutive models were enriched by non-local terms to describe strain localization properly, ensure mesh-independence in the softening regime and capture the deterministic size effect. The constitutive models were used to simulate strain localization in concrete in two boundary value problems under plane strain conditions, *viz.* uniaxial tension and three-point bending. The effect of the characteristic length on load-displacement curves and widths of strain localization is discussed.

Keywords: characteristic length, concrete, damage mechanics, elasto-plasticity, FEM, non-local model, strain localization

1. Introduction

Elasto-plastic analysis of concrete elements is a complex task due to occurrences of strain localization, a fundamental phenomenon under quasi-static and dynamic conditions [1–5]. It may occur in the form of cracks (if cohesive properties are dominant) or shear zones (if frictional properties prevail). Determination of the width and spacing of strain localization is crucial for evaluation of the material strength at the peak and in the post-peak regime. The concrete's behaviour can be modelled in continuum mechanical models using non-linear elasticity [6], fracture mechanics [7, 8], the endochronic theory [9, 10], the micro-plane theory [11, 12], elasto-plasticity [13–16], damage mechanics [17–20] and coupled plastic-damage approach [21–24], discrete models using a lattice approach [25–29] and Discrete Element Method (DEM) [30–32], *etc.* A description of strain localization requires that constitutive models must

to include strain softening. In order to describe strain localization properly in the framework of continuum mechanics, the models with softening can be enhanced with a characteristic length of the micro-structure [5]. There are several approaches within continuum mechanics to include characteristic length and regularize the ill-posedness of the underlying incremental boundary value problem [33] due to strain-softening material behaviour and localization formation (*viz.* differential equations of motion not changing their elliptic type during quasi-static calculations and their hyperbolic type during dynamic calculations), as well as avoid a pathological mesh-sensitivity of numerical solutions for quasi-brittle materials such as second-gradient [5, 18, 34], non-local [2, 16, 19, 35, 36] and viscous ones [37, 38]. Thanks to these, objective and properly convergent numerical solutions for localized deformation are achieved (a mesh-insensitive load-displacement diagram and a mesh-insensitive deformation pattern). Otherwise, FEM results are completely controlled by the size and orientation of the mesh and thus produce unreliable results, *i.e.* strain localization is narrowed upon mesh refinement (element size becomes the characteristic length) and computed force-displacement curves change considerably depending on the width of the calculated localization. Additionally, premature divergence of incremental FEM calculations occurs. The presence of a characteristic length also allows one to take into account the microscopic inhomogeneities triggering shear localization (*e.g.* grain size, size of micro-defects) and to capture the deterministic size effect of a specimen (*i.e.* the dependence of strength and other mechanical properties on the specimen's size) observed experimentally in softening granular and brittle specimens [2]. This is possible as the l_c/D ratio governs the model's response (l_c – characteristic length, D – specimen size).

The aim of the present paper is to compare results of FEM calculations of strain localization in notched concrete specimens under plane strain conditions during uniaxial tension and three-point bending. Two simple isotropic continuum models enhanced with characteristic length of microstructure were used to simulate specimens' behaviour: the elasto-plastic model and the damage model, both with non-local softening. The FEM results were quantitatively compared with laboratory experiments with respect to load-displacement curves and qualitatively – with other numerical solutions.

2. Constitutive models for concrete

2.1. The isotropic elasto-plastic model

An elasto-plastic model with isotropic hardening and softening using two yield conditions was assumed. In the compression regime, the Drucker-Prager criterion with a non-associated flow rule was defined as follows [39]:

$$f_1 = q + p\tan\varphi - \left(1 - \frac{1}{3}\tan\varphi\right)\sigma_c(\kappa_1), \qquad (1)$$

where q was the Huber-Mises equivalent stress, p – mean stress, φ – the internal friction angle, σ_c – uniaxial compression yield stress, and κ_1 – the hardening

(softening) parameter equal to plastic strain in uniaxial compression, ε_{11}^p. Invariants p and q are defined to be [40]:

$$p = \frac{1}{3}\sigma_{kk} \quad \text{and} \quad q = \sqrt{\frac{3}{2}s_{ij}s_{ji}}, \tag{2}$$

where σ_{ij} was the stress tensor and s_{ij} – the deviator of the stress tensor σ_{ij}. The slope of the yield surface has been described by the $\tan\varphi$ parameter [39]:

$$\tan\varphi = \frac{3(1-r_{bc}^\sigma)}{1-2r_{bc}^\sigma}, \tag{3}$$

wherein r_{bc}^σ was the ratio of strengths during biaxial and uniaxial compression ($1.1 \le r_{bc}^\sigma \le 1.2$). The flow potential function was taken as:

$$g_1 = q + p\tan\psi, \tag{4}$$

where ψ was the dilatancy angle ($\psi \ne \varphi$).

In the tensile regime, the Rankine criterion was assumed with the following yield function:

$$f_2 = \max\{\sigma_1, \sigma_2, \sigma_3\} - \sigma_t(\kappa_2), \tag{5}$$

where σ_1, σ_2 and σ_3 were principal stresses, σ_t – the tensile yield stress, and κ_2 – the softening parameter (equal to the maximum principal plastic strain, ε_1^p). The associated flow rule was assumed [41].

This simple constitutive isotropic elasto-plastic model for concrete, Equations (1)–(5), required two elastic parameters (*viz.* Young modulus of elasticity, E, and the Poisson ratio, v), a compression plastic function, $\sigma_c = f(\kappa_1)$, a tensile plastic function, $\sigma_t = f(\kappa_2)$, internal friction angle, φ, and dilatancy angle, ψ. The model's disadvantage was that the shape of the failure surface in the principal stress space was linear and not paraboloidal, as it is in reality. In deviatoric planes, the shape was circular (during compression) and triangular (during tension); thus, it did not change from a curvilinear triangle with smoothly rounded corners to a near circle with increasing pressure. The strength was similar for triaxial compression and extension, while the stiffness degradation due to strain localization and non-linear volume changes during loading were neglected.

2.2. The isotropic damage model

The damage variable associated with a material's degradation due to the propagation and coalescence of micro-cracks and micro-voids is defined as the ratio of the damage area to the material's overall area [40, 42, 43]. The simplest isotropic damage continuum model describes the degradation with the aid of a single scalar damage parameter, D, increasing monotonically from zero (for undamaged material) to one (for completely damaged material). The stress-strain function is represented by the following relationship:

$$\sigma_{ij} = (1-D)C_{ijkl}^e\varepsilon_{kl}, \tag{6}$$

where C_{ijkl}^e is the linear elastic material stiffness matrix and ε_{kl} – the strain tensor. The damage parameter, D, acts as a stiffness reduction factor (the Poisson ratio, ν, is not affected by damage). A general isotropic damage model should deal with two scalar parameters corresponding to two independent elastic constants. The increase

of the damage variable, D, is controlled by a damage threshold parameter, κ, defined as a maximum of the equivalent strain measure, $\tilde{\varepsilon}$, obtained during the load history up to time t. The loading function of damage is:

$$f(\tilde{\varepsilon}, \kappa) = \tilde{\varepsilon} - \max\{\kappa, \kappa_0\}, \tag{7}$$

where κ_0 is the initial value of κ. If the loading function, f, is negative, damage does not develop. Parameter κ increases during monotonic loading (coincidentally with $\tilde{\varepsilon}$) and remains constant during unloading and reloading.

Two criteria were assumed to define the equivalent strain measure, $\tilde{\varepsilon}$: (i) the Huber-Mises failure criterion in terms of strains [18] and (ii) the Rankine failure-type criterion [44].

With the former, the equivalent strain measure, $\tilde{\varepsilon}$, was [18]:

$$\tilde{\varepsilon} = \frac{k-1}{2k(1-2\nu)}I_1 + \frac{1}{2k}\sqrt{\frac{(k-1)^2}{(1-2\nu)^2}I_1^2 + \frac{12k}{(1+\nu)^2}J_2}, \tag{8}$$

where ν was the Poisson ratio, while I_1 and J_2 were respectively the first invariant of the strain tensor and the second invariant of the deviatoric strain tensor:

$$I_1 = \varepsilon_{11} + \varepsilon_{22} + \varepsilon_{33}, \quad J_2 = \frac{1}{2}\varepsilon_{ij}\varepsilon_{ij} - \frac{1}{6}I_1^2. \tag{9}$$

The k parameter of Equation (8) denotes the material's compressive/tensile strength ratio.

In the latter case, the equivalent strain measure, $\tilde{\varepsilon}$, was defined as the maximum principal effective stress scaled by the modulus of elasticity [44]:

$$\tilde{\varepsilon} = \frac{1}{E}\max\{\sigma_i^{\text{eff}}\}, \tag{10}$$

where E denoted the modulus of elasticity and σ_i^{eff} were the principal values of the effective stress,

$$\sigma_{ij}^{\text{eff}} = C_{ijkl}^e \varepsilon_{kl}. \tag{11}$$

An exponential softening law was used to describe the evolution of the damage parameter, D [18]:

$$D = 1 - \frac{\kappa}{\kappa_0}\left(1 - \alpha + \alpha e^{-\beta(\kappa - \kappa_0)}\right), \tag{12}$$

where α and β were material parameters.

The constitutive isotropic damage model for concrete requires the following parameters: E, υ, κ_0, α, β, k (Equation (8)) and E, υ, κ_0, α, β (Equation (10)). The model is suitable for tensile failure and cannot describe irreversible deformations. Neither can it realistically describe volume changes [45].

3. Non-local approach

An integral-type non-local theory was used as a regularization technique [35, 46–49] in order to describe strain localization properly, preserve the well-posedness of the boundary value problem, obtain FEM results free from spurious discretization sensitivity and capture the deterministic size effect (dependence of the nominal strength on the structure size). It was achieved with weighted spatial averaging over the neighbourhood of each material point of a suitable state variable. Thus, stress at

a certain material point depended not only on the state variable at that point, but also on the distribution of state variables in a finite neighbourhood of the point considered. (The principle of local action did not hold – non-local interaction took place between any two points). Elasto-plastic models of this kind were developed by Bazant and Lin [47], Brinkgreve [48] and others. Damage models of this kind were first proposed by Pijaudier-Cabot and Bazant [35]. It is usually sufficient to treat non-locally only one variable controlling material softening or degradation [35], whereas stresses and strains remain local.

It was assumed in our elasto-plastic model that the softening parameter, κ_i, was non-local only:

$$\bar{\kappa}_i(x_k) = \frac{1}{A} \int \omega(r) \kappa_i(x_k + r) \, dV, \tag{13}$$

where x_k were the coordinates of the considered (actual) point, r – distance measured from point x_k to other material points, ω – the weighting function, and A – weighted volume. The Gauss distribution function was used as the weighting function, ω (which is usually non-negative and normalized):

$$\omega(r) = \frac{1}{l_c \sqrt{\pi}} e^{-\left(\frac{r}{l_c}\right)^2}, \tag{14}$$

where l_c denoted a characteristic (internal) length controlling the spread of the non-local weight function. The averaging in Equation (13) is restricted to a small representative area around each material point. The influence of the points at the distance of $r = 3l_c$ is merely about 0.1%. Characteristic length can be related to the material's micro-structure (*e.g.* aggregate size in concrete). According to Pijaudier-Cabot and Bazant [35] and Bazant and Oh [49], it is approximately $3 \times d_a$ in concrete, where d_a is the maximum aggregate size. It is usually determined in an inverse identification process of experimental data [50, 51] since it cannot be measured directly. Le Bellego *et al.* [52] have recently presented a calibration method of non-local models including characteristic length on the basis of 3 size effect bending tests. However, to determine one representative characteristic length of a micro-structure is very difficult in concrete, where strain localization can include a mixed mode (cracks and shear zones [42]) and characteristic length, although one-dimensional, is related to the fracture process zone of a certain area or volume [42] which increases during deformation (*e.g.* on the basis of acoustic emission measurements of Pijaudier-Cabot *et al.* [53]). Other researchers have concluded that characteristic length is not a constant and it depends on the type of the boundary value problem and the current level of damage [54]. Thus, a determination of l_c requires further numerical analyses and measurements, *e.g.* using a differential interference contrast DIC technique [55]. Measurements of load-displacement curves and width of the fracture process zone in experiments with the same concrete for different boundary value problems and specimen sizes are particularly important [56].

The softening rates, $d\kappa_i$, Equations (1) and (5), were assumed to be a linear combination of the local and non-local values (independently for both yield surfaces)

according to the modified Brinkreve formula [48] (the so-called over-non-local formu-
lation):

$$d\bar{\kappa}_i(x_k) = (1-m)\,d\kappa_i(x_k) + \frac{m}{A}\int \omega(r)\,d\kappa_i(x_k+r)\,dV, \tag{15}$$

where m was the non-local parameter, which should be greater than 1 to obtain
mesh-independent results [16, 57]. Equation (15) can be rewritten as follows [48]:

$$d\bar{\kappa}_i(x_k) = d\kappa_i(x_k) + m\left(\frac{1}{A}\int \omega(r)\,d\kappa_i(x_k+r)\,dV - d\kappa_i(x_k)\right). \tag{16}$$

Since the rate of the hardening parameter was unknown at the beginning of each
iteration, additional sub-iterations are required to solve Equation (16). To simplify
the calculations, the non-local rates were replaced with their approximations, $d\kappa_i^{\mathrm{est}}$,
calculated on the basis of the known total strain rates [16]:

$$d\bar{\kappa}_i(x_k) \approx d\kappa_i(x_k) + m\left(\frac{1}{A}\int \omega(r)\,d\kappa_i^{\mathrm{est}}(x_k+r)\,dV - d\kappa_i^{\mathrm{est}}(x_k)\right). \tag{17}$$

In the damage mechanics model, the equivalent strain measure, $\tilde{\varepsilon}$, of Equations (8)
and (10) was replaced with its non-local definition, $\bar{\varepsilon}$ (the response was local in the
elastic range):

$$\bar{\varepsilon}(x_k) = \frac{1}{A}\int \omega(r)\,\tilde{\varepsilon}(x_k+r)\,dV. \tag{18}$$

4. Implementation

Both models, enhanced by non-local terms, were implemented in the Abaqus
commercial finite element code [39] for efficient computations. Such implementation
can be performed with two methods.

In one method, two identical overlapping meshes are used. One mesh enables
obtaining information about coordinates of integration points in the entire specimen,
area of all finite elements and total strain rates in each element. The elements in this
mesh are defined by the user in the UEL procedure. As they have no stiffness, they have
no influence on the stress results for the specimen's body. The stored information is
needed to calculate non-local variables with the aid of the other mesh, which includes
standard elements from the Abaqus library. The constitutive law is defined by the
UMAT procedure. During odd iterations, information is gathered in the elements of
the first mesh. During even iterations, the stresses in the elements of the second mesh
(including standard elements) are determined taking into account non-local variables
and a non-linear finite element equation is solved. Between odd and even iterations,
the same element configuration is imposed.

In the other method, only one mesh is used, which contains the user's elements
(defined by the UEL procedure). Information about elements is stored during odd
iterations and stresses within a non-local theory are determined during even iterations.
This method consumes less time, but it is not so user-friendly as it requires defining
the stiffness matrix and out-of-balance load vector in finite elements.

A modified Newton-Raphson scheme was used to solve the non-linear equation
of motion governing the response of a system of finite elements. The calculations
were performed with a symmetric elastic global stiffness matrix. Calculations with

a full Newton-Raphson method resulted in poor convergence in the softening regime, as determination of a tangent stiffness matrix within a non-local theory is virtually impossible. The following convergence criteria were assumed [39]:

$$r_{\max} \le 0.01\tilde{q} \quad \text{and} \quad c_{\max} \le 0.01\Delta u_{max}, \tag{19}$$

where $r_{\max}$ was the largest residual out-of-balance force, $\tilde{q}$ – the spatial force averaged over the entire body, $c_{\max}$ – the greatest correction of the displacement, and $\Delta u_{\max}$ – the greatest change of displacement in an increment. The procedure yielded sufficiently accurate and fast convergence. The magnitude of the maximum out-of-balance force at the end of each calculation step was less than 1% of the calculated total vertical force at the specimen's top. Calculations with smaller tolerances (see Equation (19)) did not influence the FEM results. Integration was performed in one sample point of each element (centroid).

To satisfy the consistency condition, $f = 0$, the trial stress method (linearized expansion of the yield condition about the trial stress point) using an elastic predictor and a plastic corrector with return mapping algorithm (see [58]) was applied with the following criterion:

$$r_\lambda/\sigma_y^{\max} \le 10^{-6}, \tag{20}$$

where r_λ was the residual plastic multiplier and $\sigma_y^{\max}$ denoted the maximum cohesion yield stress in each increment.

The calculations were carried out using large-displacement analysis available in the Abaqus finite element code [39]. In this method, the body's actual configuration was taken into account. The Cauchy stress was taken as the stress measure. The conjugate strain rate was the rate of deformation. Rotation of the stress and strain tensor was calculated with the Hughes-Winget [59] method. Non-local averaging was performed in the current configuration.

5. FEM simulations

5.1. Uniaxial tension

The problem of a symmetric double-notched concrete specimen under uniaxial tension was experimentally investigated by Hordijk [60]. The geometry of his concrete specimen (width $b = 60$ mm, height $h = 125$ mm, thickness in the out-of-plane direction $t = 50$ mm) and boundary conditions are presented in Figure 1. Two symmetric notches
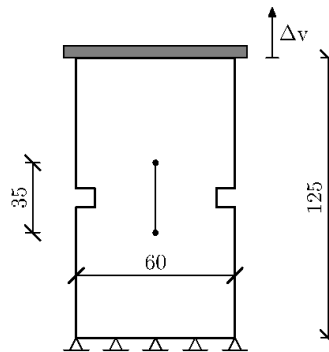

Figure 1. Geometry and boundary conditions of a specimen with a notch under uniaxial tension (dimensions given in mm)
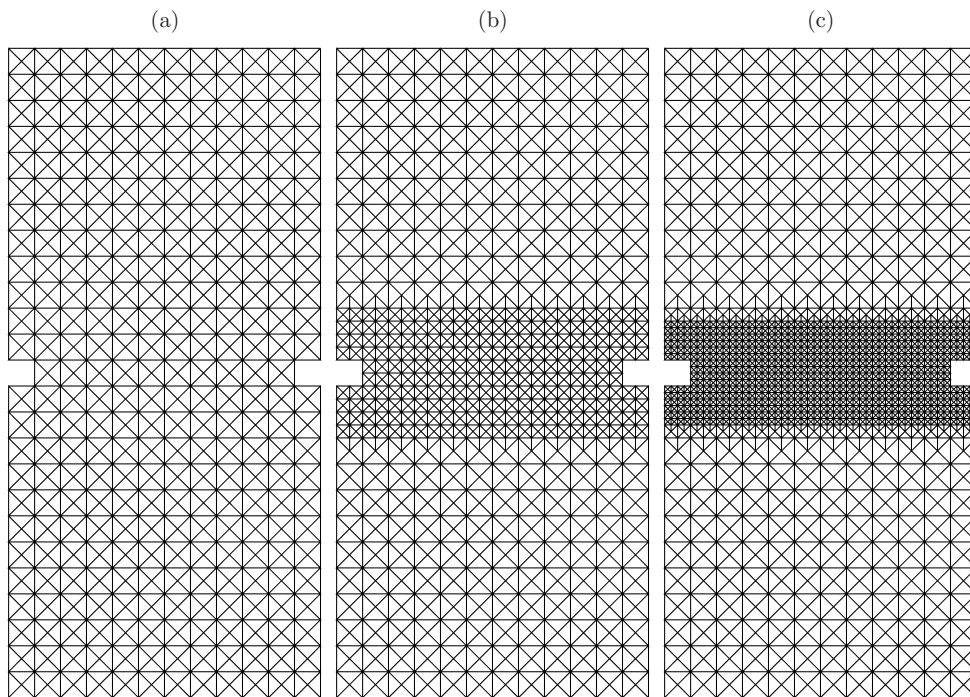
(a)   (b)   (c)

Figure 2. FE meshes used for calculations of uniaxial tension: (a) coarse, (b) medium, (c) fine
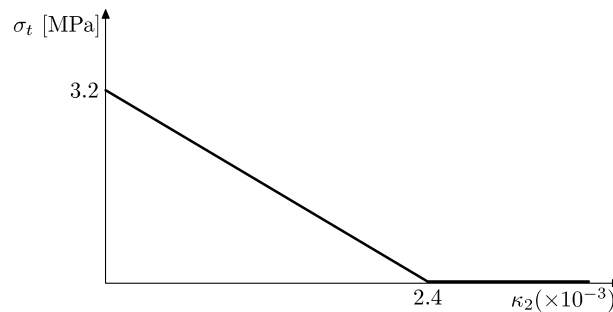

Figure 3. Assumed $\sigma_t = f(\kappa_2)$ curve in the tensile regime/elasto-plastic model for uniaxial tension with softening modulus $H_t = 2300$MPa (σ_t – tensile plastic stress, κ_2 – softening parameter)

5×5mm^2 each were located at the mid-point of both of the specimen's sides. Three different FE meshes were used: coarse (1192 triangular elements), medium (1912 triangular elements) and fine (4168 triangular elements), see Figure 2. The so-called „shading effect" was considered when calculating non-local quantities close to the notch (*i.e.* the averaging procedure considered the notch as an internal barrier shading non-local interaction [61]).

The modulus of elasticity was equal to $E = 18.0$GPa, Poisson's ratio was $\upsilon = 0.2$ and the tensile strength was $f_t = 3.2$MPa in both models.

The elasto-plastic calculations were carried out with 3 different diagrams describing the tensile plastic stress, σ_t, versus the softening parameter, κ_2. A linear
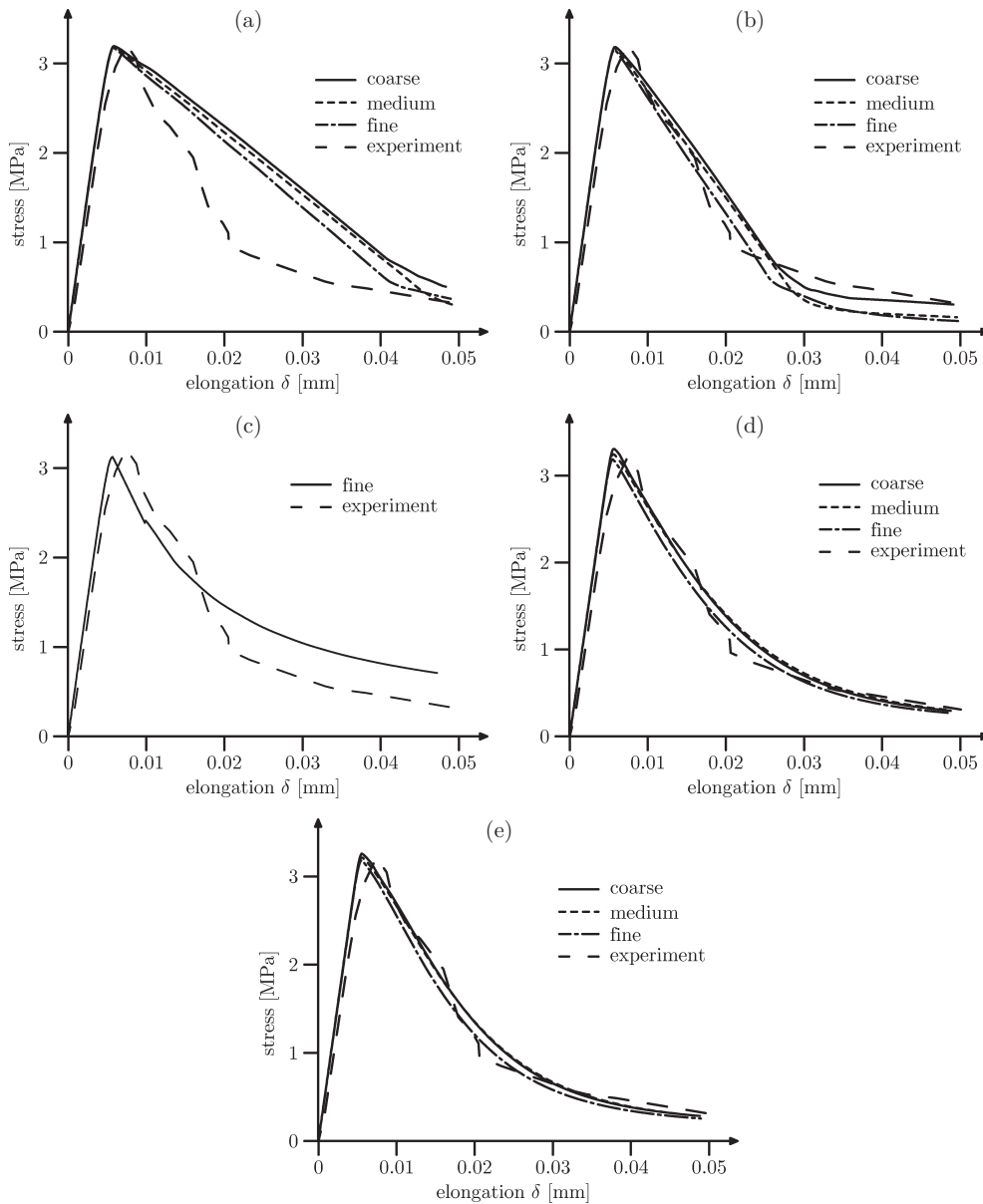
Figure 4. Calculated stress-elongation diagrams for a specimen under uniaxial tension with various FE meshes compared with the experimental diagram [60]: (a) the elasto-plastic model with non-local linear softening (softening modulus $H_t = 1300$MPa), (b) the elasto-plastic model with non-local linear softening $H_t = 2300$MPa), (c) the elasto-plastic model with non-local exponential softening with Equation (21), (d) the damage model with non-local softening, Equation (8), (e) the damage model with non-local softening, Equation (10)

and non-linear $\sigma_t = f(\kappa_2)$ relationship was assumed in the softening tensile regime. In the case of linear softening, two softening modules were used: $H_t = 3.2/(2.4 \cdot 10^{-3}) \approx 1300$MPa (Figure 3) and $H_t = 3.2/(1.5 \cdot 10^{-3}) \approx 2100$MPa. Additionally, a curvilinear exponential softening curve proposed by Hordijk [60] was taken into account in the tensile regime:
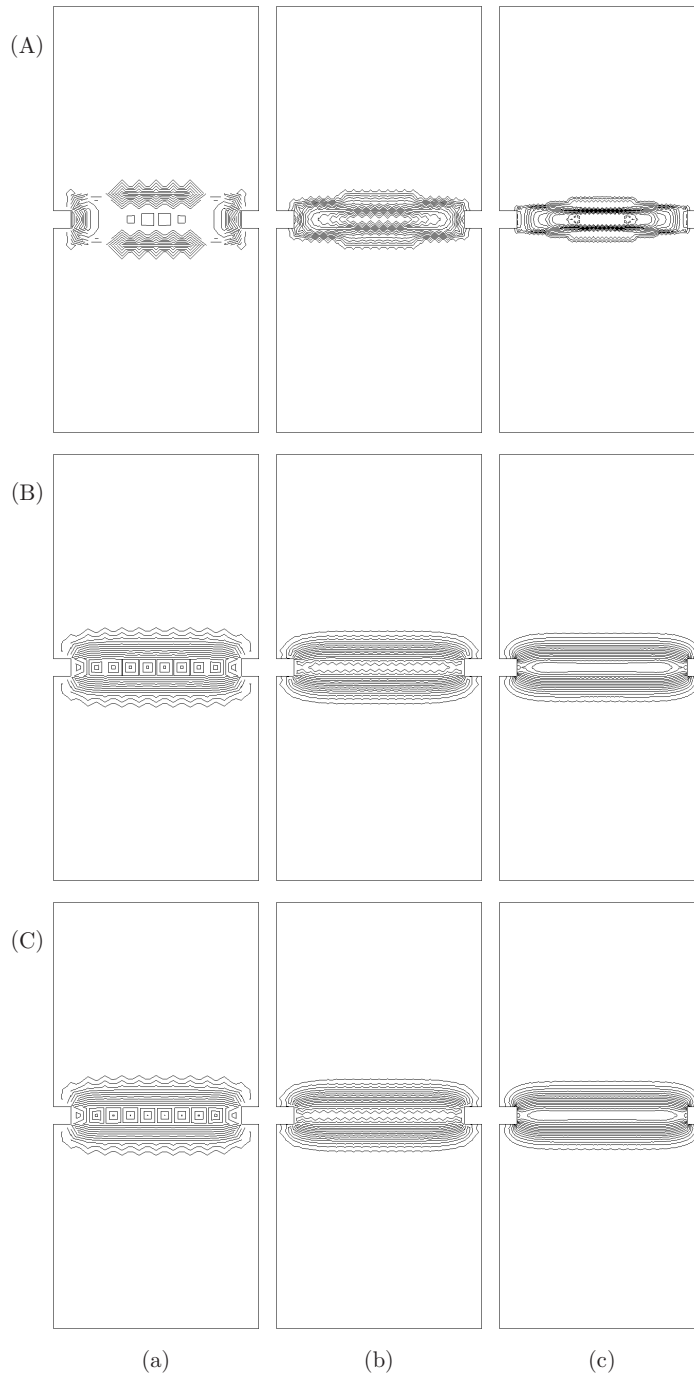
Figure 5. Calculated contours of non-local parameter $\bar{\kappa}_2$ in a specimen under uniaxial tension for (a) coarse, (b) medium and (c) fine mesh: (A) the elasto-plastic model with non-local softening (softening modulus $H_t = 1300\,\mathrm{MPa}$), (B) the damage model with non-local softening, Equation (8), (C) the damage model with non-local softening, Equation (10)

$$\sigma_t(\kappa_2) = f_t \left\{ \left[1 + \left(c_1 \frac{\kappa_2}{\kappa_u} \right)^3 \right] \exp\left(-c_2 \frac{\kappa_2}{\kappa_u} \right) - \frac{\kappa_2}{\kappa_u} \left(1 + c_1^3 \right) \exp(-c_2) \right\}, \quad (21)$$

where κ_u was the ultimate value of the softening parameter ($\kappa_u = 0.007$) and c_1, c_2 were constants equal to 3 and 6.93, respectively [60]. The non-locality parameter $m = 2$ was chosen on the basis of initial own FE studies [16] and studies presented in [57]. Higher values of m resulted in unrealistically large strain localization widths.

The following parameters were chosen for the damage models: $\kappa_0 = 2.2 \cdot 10^{-4}$, $\alpha = 0.96$, $\beta = 600$ and $k = 10$ (Equations (8) and (12)) and $\kappa_0 = 1.7 \cdot 10^{-4}$, $\alpha = 0.96$ and $\beta = 900$ (Equations (10) and (12)).

The characteristic length, l_c, was assumed to be 5 mm in both models, on the basis of initial calculations with non-local models [16, 22, 62].

The nominal stress-elongation tensile curves for all the meshes, are shown in Figure 4 in comparison with the experimental curve [60]. The elongation δ of Figure 4 denotes the specimen's elongation above and below both notches at the height of 35 mm (*cf.* Figure 1). It was measured experimentally by 4 pairs of extensometers with a gauge length of 35 mm [60]. The vertical normal stress was calculated by dividing the calculated resultant vertical force by the specimen cross-section of 50×50 mm^2. The calculated load-displacement curves of Figure 4 practically coincide for the different meshes and models (in particular for damage models). They are also in satisfactory agreement with the experimental curve (especially the damage curves and the elasto-plastic curve with linear softening under $H_t = 2100$ MPa), although a small deviation between the theory and the experiment has occurred (*cf.* [60]).

The calculated contours of the $\bar{\kappa}_2$ non-local parameter in the specimen are shown in Figure 5 in the residual state for $\delta = 0.05$ mm. The width of the localization zone between two notches (w_{lz}, determined from the distribution of $\bar{\kappa}_2$) is similar for both damage models, $w_{lz} = 25$ mm ($5.0 \times l_c$). In elasto-plasticity, the width of the localization zone is approximately 25 mm for the coarse mesh, 20 mm for the medium mesh and 15 mm ($3.0 \times l_c$) for the fine mesh and is not influenced by the rate of softening (Figure 6).

Additionally, the influence of the micro-structure's characteristic length, l_c, on the specimen's behaviour was investigated. FEM calculations were performed with l_c in the range from 2.5 mm to 10.0 mm using the mesh shown in Figure 2c. The obtained load-displacement curves are presented in Figure 7. The greater the characteristic length (up to $l_c = 7.5$ mm), the higher the maximum tensile stress. The slope to the horizontal of all curves after the peak decreases with increasing l_c (the material becomes more ductile with increasing l_c). The calculated contours of the non-local parameter κ in the specimen are shown in Figure 8 in the residual state for a fine mesh shown in Figure 2c. In general, the width of the localized zone, w_{lz}, increased with increasing l_c; it was 10 mm ($4.0 \times l_c$ for $l_c = 2.5$ mm) or 15 mm ($3.0 \times l_c$ for $l_c = 5$ mm, $2.0 \times l_c$ for $l_c = 7.5$ mm and $1.5 \times l_c$ for $l_c = 10$ mm) using the elasto-plastic model, and 15 mm ($6.0 \times l_c$ for $l_c = 2.5$ mm), 25 mm ($5.0 \times l_c$ for $l_c = 5$ mm) or 35 mm ($4.7 \times l_c$ for $l_c = 7.5$ mm and $3.7 \times l_c$ for $l_c = 10$ mm) using the damage model, Equation (8).

The results are in good qualitative accordance with the FEM results obtained by Gutierrez and de Borst [63] with the second-gradient elasto-plastic model and those of Peerlings *et al.* [18] and Pamin [64], using the second-gradient damage model, with
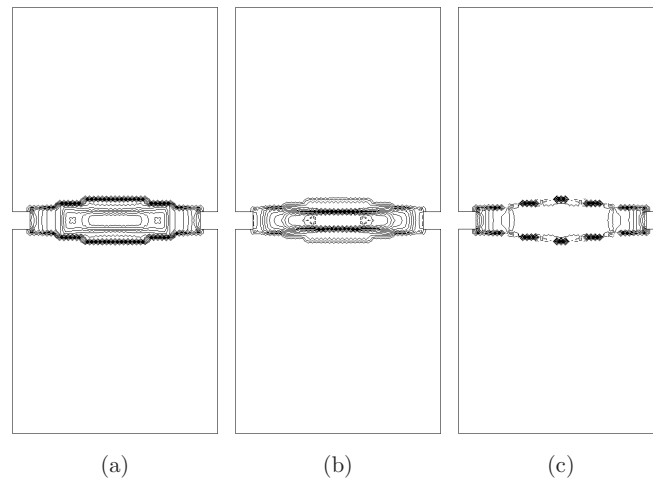
<div align="center">(a)   (b)   (c)</div>

Figure 6. Calculated contours of non-local parameter $\bar{\kappa}_2$ in a specimen under uniaxial tension for fine mesh in elasto-plasticity with non-local softening: (a) linear softening $H_t = 1300\,\text{MPa}$, (b) linear softening $H_t = 2300\,\text{MPa}$, (c) curvilinear softening with Equation (21)
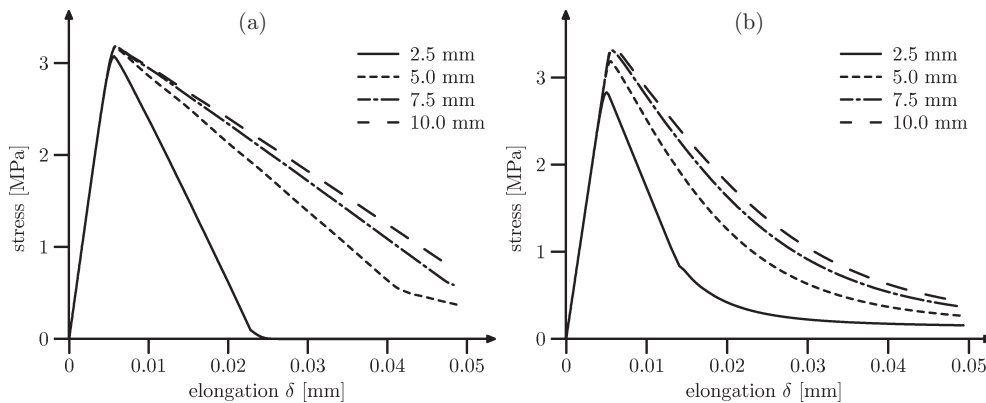

Figure 7. Calculated vertical stress-elongation diagrams using various characteristic lengths, l_c, for a specimen under uniaxial tension using a fine mesh: (a) the elasto-plastic model with non-local softening $H_t = 1300\,\text{MPa}$, (b) the damage model with non-local softening, Equation (8)

respect to the effect of characteristic length on the width of strain localization and the load-displacement curve.

5.2. Three-point bending

The behaviour of a symmetric concrete beam with a notch at the bottom at mid-span and free ends during three-point bending was simulated. It was experimentally investigated by Le Bellego *et al.* [52] and later numerically simulated by Le Bellego *et al.* [52] and Rodriguez-Ferran *et al.* [65] in a non-local damage approach. Three beams were used in laboratory tests: small ($h = 8\,\text{cm}$), medium ($h = 16\,\text{cm}$) and large ($h = 32\,\text{cm}$). The beam span was $L = 3h$. The beam's geometry and boundary conditions are presented in Figure 9. The loading was prescribed at the top edge's mid-span through vertical displacement.
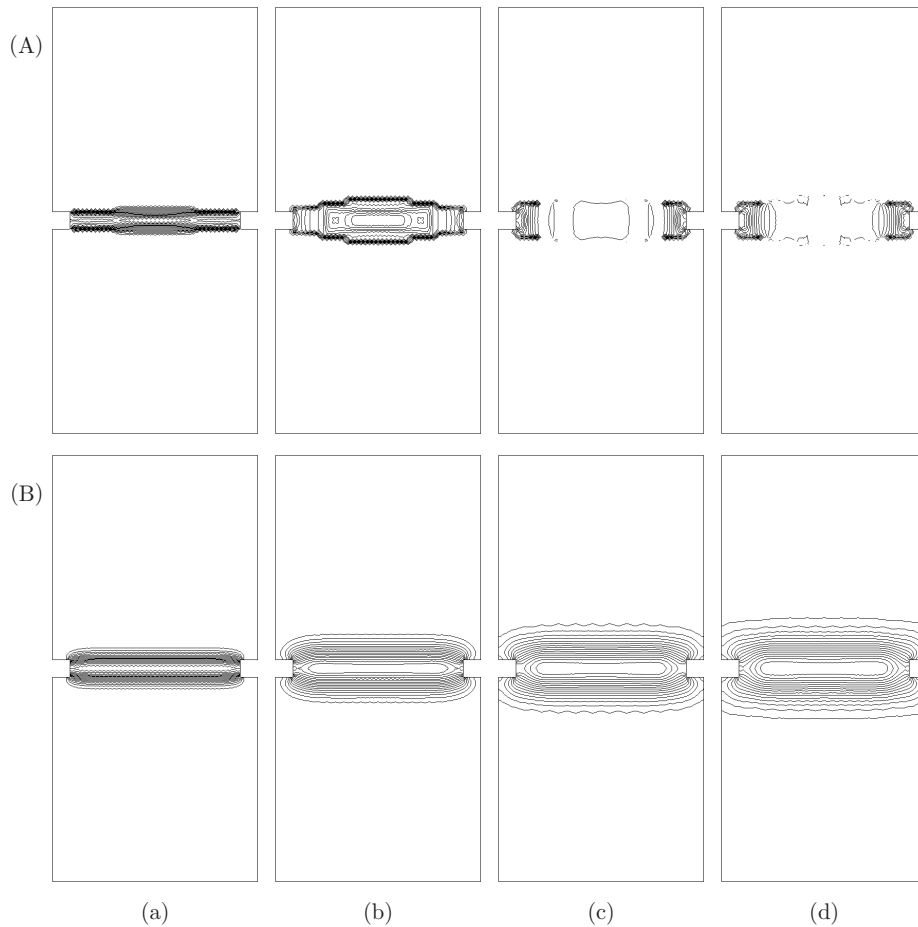
Figure 8. Calculated contours of damage parameter $\bar{\kappa}_2$ in a specimen under uniaxial tension for a fine mesh of (a) $l_c = 2.5$mm, (b) $l_c = 5$mm, (c) $l_c = 7.5$mm, (d) $l_c = 10$mm: (A) the elasto-plastic model with non-local softening, (B) the damage model with non-local softening, Equation (8)
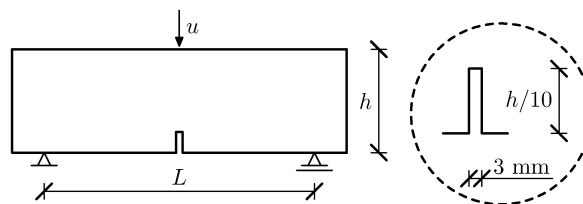

Figure 9. Geometry of the beam and boundary conditions [52]

Three FE meshes were assumed, with 1534, 2478 and 4566 triangular elements respectively for the small, medium and large specimens (see Figure 10). Due to the the problem's symmetry, only the left half of the beam was modelled.

The modulus of elasticity was assumed as E=38.5 GPa and the Poisson ratio as $\nu = 0.2$. In the tensile regime of the elasto-plastic model, the Rankine criterion with Hordijk's exponential curve was assumed with $c_1 = 3$ and $c_2 = 6.93$ (see [52], Equation (21)). Two internal lengths were chosen for the FE analysis: $l_c = 5$mm
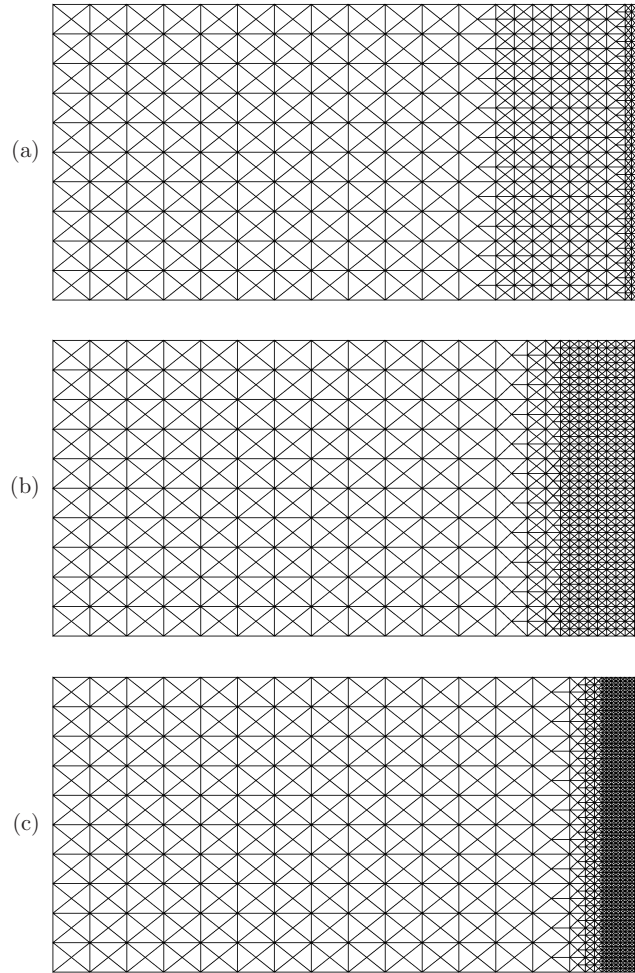
Figure 10. FE meshes used for bending calculations: (a) coarse, (b) medium, (c) fine (the damage model with non-local softening)

and $l_c = 10$mm. With two different values of l_c, two sets of material parameters were chosen for Equation (21) (with $m = 2$), $f_t = 3.6$MPa, $\kappa_u = 0.005$ for $l_c = 5$mm and $f_t = 3.3$MPa, $\kappa_u = 0.003$ for $l_c = 10$mm, in order to obtain the best agreement between the load-displacement diagrams from FE analyses and laboratory tests [52]. The internal friction angle equalled $\varphi = 10°$, Equation (3), and the dilatancy angle – $\psi = 5°$. The compressive strength was equal to $f_c = 40$MPa. A linear softening modulus under compression was $H_c = 0.8$MPa. However, the effect of material parameters under compression on the FEM results was insignificant.

In the damage model, Equation (10), two sets of material parameters were again chosen for two different values of l_c: $\kappa_0 = 7\cdot10^{-5}$, $\alpha = 0.99$, $\beta = 600$ for $l_c = 5$mm and $\kappa_0 = 6.25\cdot10^{-5}$, $\alpha = 0.99$, $\beta = 1000$ for $l_c = 10$mm.

Load-displacement curves for all beams obtained from FEM calculations using the internal lengths of $l_c = 5$mm and $l_c = 10$mm are compared with experiments
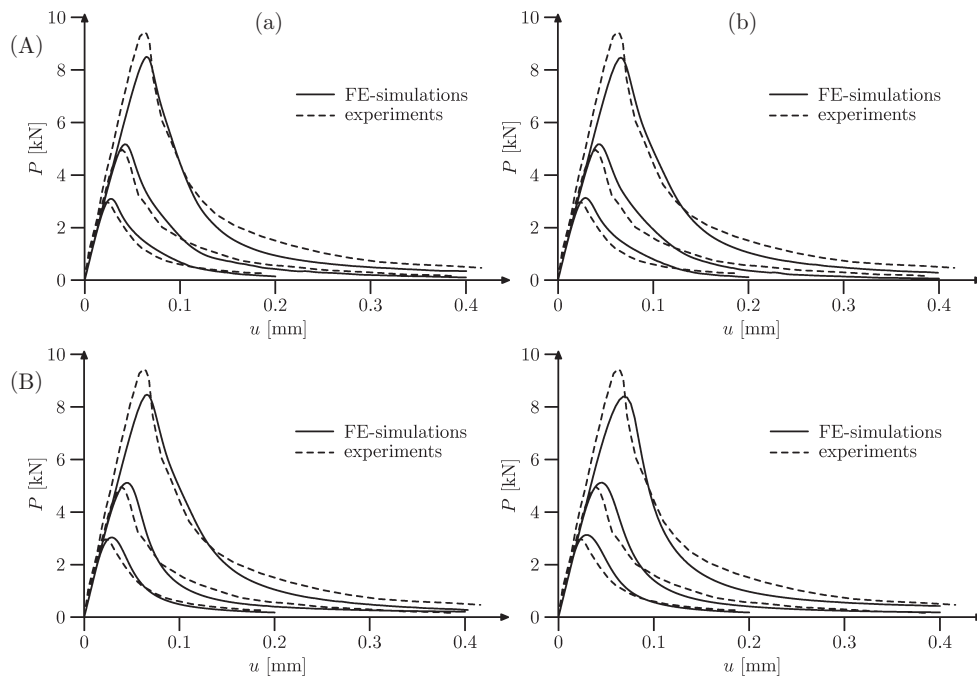
Figure 11. Load-displacement curves from experiments [52] and FEM simulations for (a) $l_c = 5$ mm, (b) $l_c = 10$ mm: (A) the elasto-plastic model with non-local softening, (B) the damage model with non-local softening, Equation (10)

in Figure 11. Satisfactory agreement with experiment has been achieved. The FEM results slightly overestimate the load bearing capacity of the small and medium beam and underestimate the maximum load for the large beam. The large to medium beam specimen strength ratio is similar to the medium to small one. The same numerical results were obtained by Le Bellego *et al.* [52] and Rodriguez-Ferran *et al.* [65], though they used different definitions of equivalent strain $\tilde{\varepsilon}$ and evolution laws. Other calculations demonstrate that the greater the characteristic length, the strober the beam, in particular in damage mechanics [20, 41].

The distribution of the $\bar{\kappa}_2$ non-local parameter above the notch is shown in Figures 12 and 13. The width of the localization zone, $\boldsymbol{w}_{lz}$, in the residual state in elasto-plasticity was about 25 mm ($5 \times l_c$) for $l_c = 5$ mm (all beams), or 50 mm ($5 \times l_c$, small and medium beams), and 45 mm ($4.5 \times l_c$, large beam) for $l_c = 10$ mm. In the damage model, it equalled 40 mm ($8 \times l_c$) for $l_c = 5$ mm, or 65 mm ($6.5 \times l_c$, small beam), 75 mm ($7.5 \times l_c$, medium beam) and 90 mm ($9 \times l_c$, large beam) for $l_c = 10$ mm. It was independent of the mesh size.

The localized zone's evolution during deformation is shown in Figure 14. The width of the localized zone increases in the early stages of deformation after the peak and remains almost unaltered during advanced deformation in elasto-plasticity. However, it increases continuously in damage mechanics. This outcome is in accordance with the FEM calculations of Pamin [64, 66], who used second-gradient elasto-plastic and damage models.
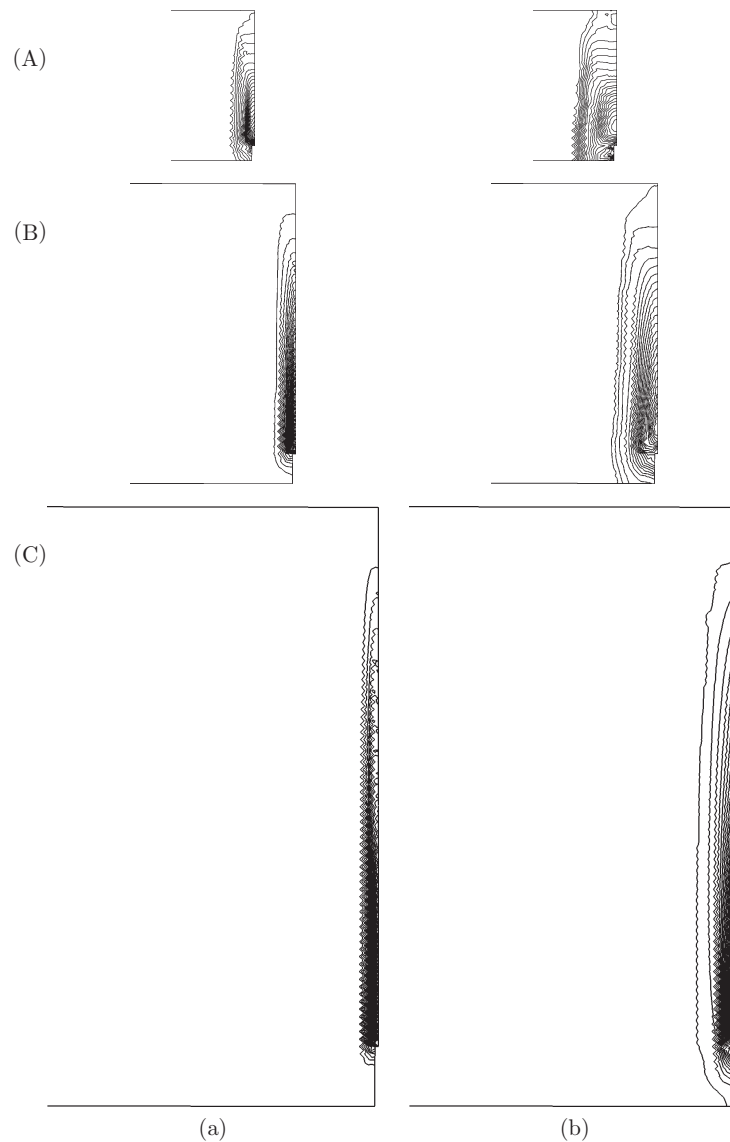
Figure 12. Calculated contours of non-local parameter $\bar{\kappa}_2$ along the beam's height at the left side of notch: (a) $l_c = 5$ mm, (b) $l_c = 10$ mm; (A) $h = 80$ mm, (B) $h = 160$ mm, (C) $h = 320$ mm (the elasto-plastic model with non-local softening)

Finally, the influence of parameters α, β and κ_0 on the force-displacement curve is shown in Figure 15 for the damage model, Equation (10). Parameter κ_0 strongly influences the peak on the load-displacement curve. The β parameter affects the slope of the curve in the softening regime while the α parameter has a considerable effect on the residual value.

6. The size effect

The size effect is the dependence of structural strength on the structure's size. The maximum normalized loads obtained from FEM simulations for notched
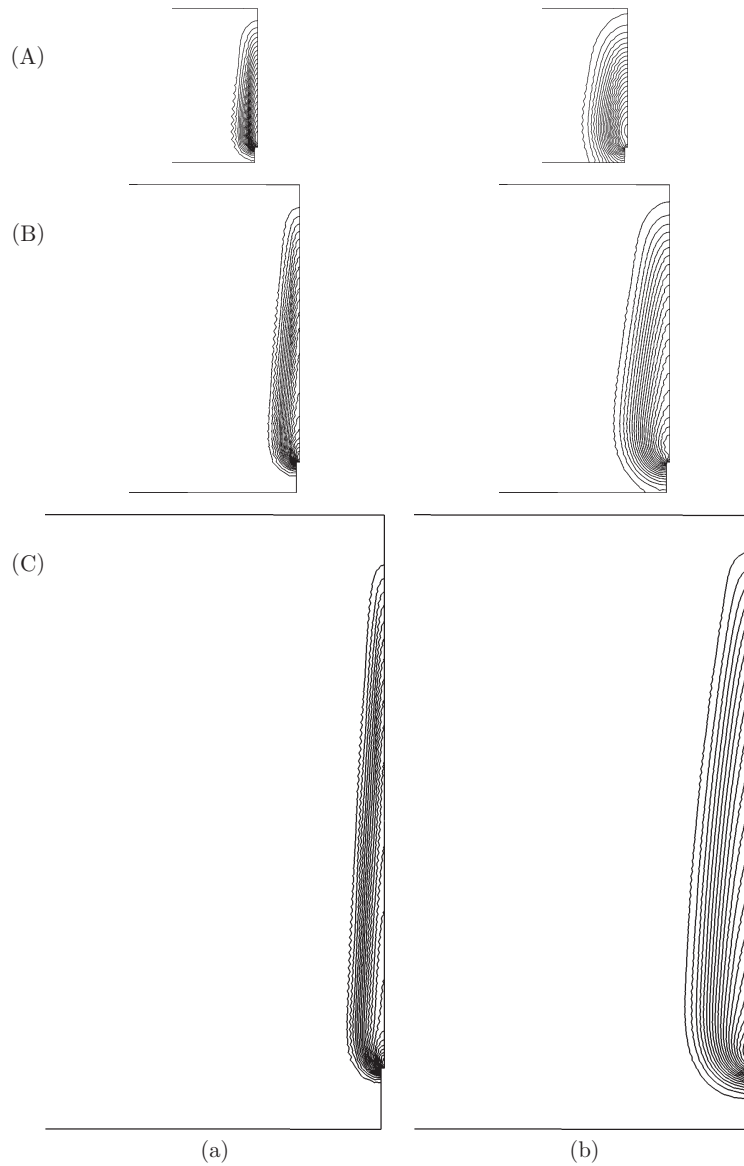
Figure 13. Calculated contours of non-local parameter $\bar{\kappa}_2$ along the beam's height at the left side of notch: (a) $l_c = 5$ mm, (b) $l_c = 10$ mm; (A) $h = 80$ mm, (B) $h = 160$ mm, (C) $h = 320$ mm (the damage model with non-local softening, Equation (10))

concrete specimens in the damage and elasto-plastic approaches (uniaxial tension and three-point bending) were compared with a deterministic (energetic) size effect law given by Bazant for structures with pre-existing notches or large stress-free cracks growing in a stable manner prior to the maximum load [2]:

$$\sigma = \frac{Bf_t}{\sqrt{1 - D/D_0}}, \tag{22}$$

where σ was nominal strength, B – a dimensionless geometry-dependent parameter (dependent on the geometry of the structure and the crack), D – specimen size and
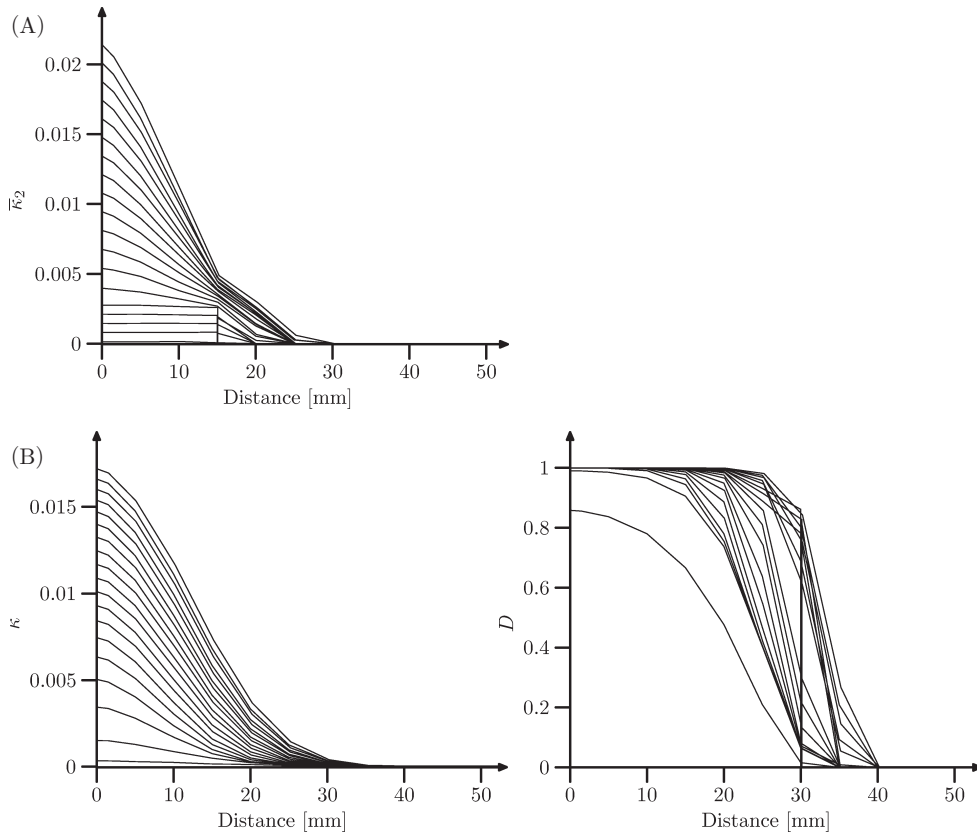
Figure 14. Evolution of non-local parameter $\bar{\kappa}_2$ and damage parameter D above the notch (the right side of the beam, $l_c = 10\,\text{mm}$, $h = 160\,\text{mm}$): (A) the elasto-plastic model with non-local softening, (B) the damage model with non-local softening, Equation (10)

D_0 – a size-dependent parameter referred-to as transitional size. Equation (22) can be rewritten as:

$$\frac{1}{\sigma^2} = \alpha D + c \quad \text{with} \quad \alpha = c/D_0 \quad \text{and} \quad B f_f = 1/\sqrt{c}. \tag{23}$$

Linear regression was used in order to find parameters B and D_0 from FE analyses. A comparison of FEM results and Bazant's size effect law [2] is presented in Figure 16: good agreement has been obtained. The normalized strength decreases almost linearly in the considered range with the increasing h/l_c size ratio.

7. Final remarks

The FEM calculations have shown that both simple isotropic constitutive models, elasto-plastic and damage with non-local softening, are capable of properly capturing the localization of strain and the related size effect in concrete. The obtained FEM results are unaffected by mesh sensitivity as the width of strain localization is determined by a characteristic length incorporated in the model. Satisfactory agreement between numerical simulations and laboratory experiments for notched concrete specimens during uniaxial tension and three-point bending has been achieved with respect to load-displacement curves.
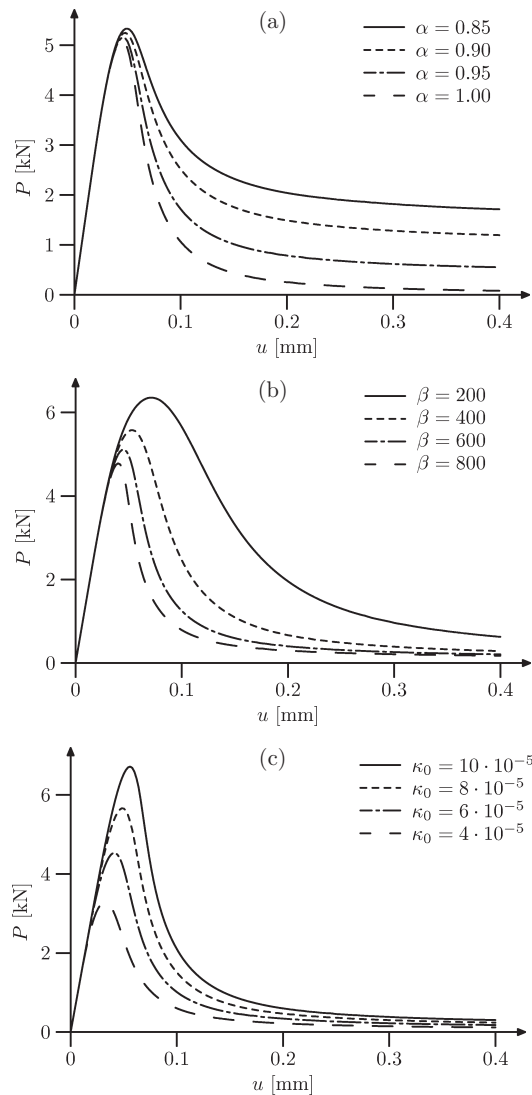
Figure 15. Influence of parameters α, β and κ_0 on the load-displacement curve
in the damage model ($l_c = 5\,\text{mm}$, $h = 160\,\text{mm}$, Equation (10))

The greater the ratio between the micro-structure's characteristic length and the specimen's size, the higher the specimen's strength and the ductility tend to be.

The width of the localized strain zone in concrete specimens increases with the increasing ratio of the micro-structure's characteristic length to the specimen's size. The increase is more pronounced in damage mechanics.

The localized zone is wider in FE analyses with the damage model than with the elasto-plastic model of similar l_c. For uniaxial tension, the width of the localized strain zone is about $(1.5 - 4.0) \times l_c$ in the elasto-plastic model and $(3.7 - 6.0) \times l_c$ in damage mechanics. For bending, the width of the localized strain zone is about $(4.5 - 5.0) \times l_c$ in elasto-plasticity and $(6.5 - 9.0) \times l_c$ in damage mechanics. The width of the localized zone is independent of the rate of softening in elasto-plasticity.
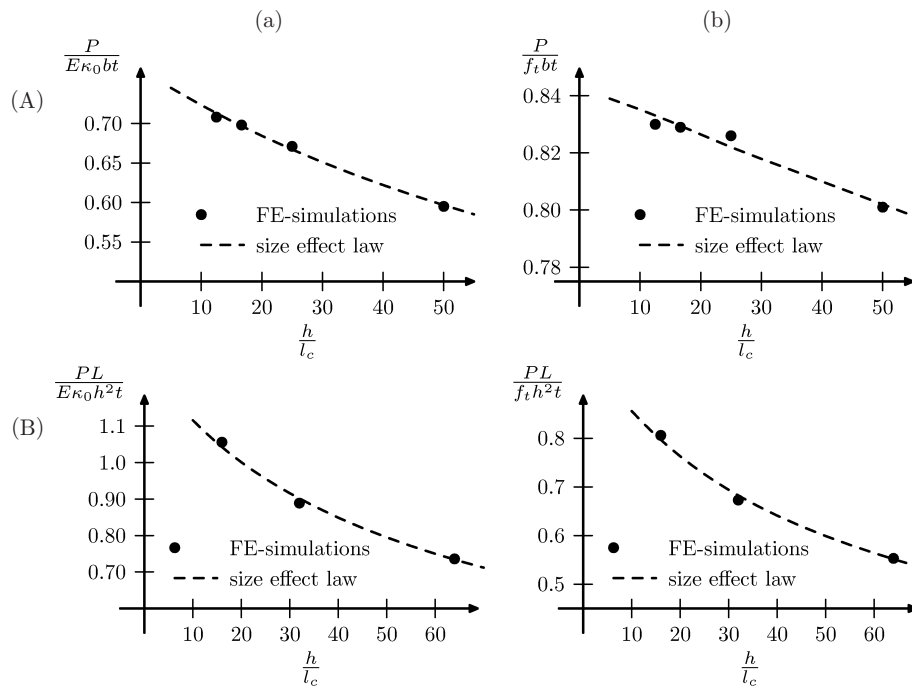
Figure 16. Relationship between calculated normalized loads (A) $P/(E\kappa_0 bt)$ and $P/(f_t bt)$ during uniaxial tension and (B) $(PL)/(E\kappa_0 h^2 t)$ and $(PL)/(f_t h^2 t)$ during bending (with $l_c = 5\,\mathrm{mm}$) and the h/l_c ratio compared with Bazant's size effect law [2] in: (a) damage mechanics and (b) elasto-plasticity

The width of the localized zone increases throughout the deformation process in damage mechanics, whereas it is almost constant in elasto-plasticity.

The calculated deterministic size effect in notched concrete elements during tension and bending is in agreement with the corresponding size effect law of Bazant [2].

In order to identify the characteristic length of a micro-structure, FEM simulations of different laboratory experiments with the same concrete are necessary, wherein the load-displacement curve and the displacement field are measured simultaneously.

Our calculations on strain localization in concrete will be continued. The damage model with non-local softening will be combined with an elasto-plastic hardening model to include plastic deformations [56, 57], first using the Drucker-Prager failure criterion, Equation (1), and then the Menetrey and Willam criterion [15]. Afterwards, anisotropy will be included in the model [67]. Spatially correlated distribution of the tensile strength will be assumed in order to describe an effect of statistical size [68, 69]. Additionally, laboratory tests will be performed wherein the width of the fracture process zone will be measured using a DIC technique [70].

Acknowledgements

References

[1] Bazant Z P 1984 *Size effect in blunt fracture: concrete, rock, metal, J. Eng. Mech. ASCE* **110** 518

[2] Bazant Z P 2003 *Scaling of Structural Strength*, Hermes-Penton, London

[3] Wittmann F H, Mihashi H and Nomura N 1992 *Size effect on fracture energy using three-point bend tests, Mater. Struct.* **25** 327

[4] van Vliet M R A and van Mier J G M 1996 *Experimental investigation of concrete fracture under uniaxial compression, Mech. Cohesive-Frictional Mater.* **1** 115

[5] Chen J, Yuan H and Kalkhof D 2001 *A nonlocal damage model for elastoplastic materials based on gradient plasticity theory, Report Nr. 01–13*, Paul Scherrer Institut, pp. 1–130

[6] Palaniswamy R and Shah S P 1974 *Fracture and stress-strain relationship of concrete under triaxial compression, J. Struct. Div. ASCE* **100** 901

[7] Bazant Z P and Cedolin L 1979 *Blunt crackband propagation in finite element analysis, J. Eng. Mech. Div. ASCE* **105** (2) 297

[8] Hilleborg A 1985 *The theoretical basis of a method to determine the fracture energy of concrete, Mater. Struct.* **18** 291

[9] Bazant Z P and Bhat P D 1976 *Endochronic theory of inelasticity and failure of concrete, J. Eng. Mech. Div. ASCE* **102** 701

[10] Bazant Z P and Shieh C L 1978 *Endochronic model for nonlinear triaxial behaviour of concrete, Nucl. Eng. Des.* **47** 305

[11] Bazant Z P and Ozbolt J 1990 *Non-local microplane model for fracture, damage and size effect in structures, J. Eng. Mech. ASCE* **116** 2485

[12] Jirasek M 1999 *Comments on microplane theory, Mechanics of quasi-brittle materials and structures* (Pijaudier-Cabot G, Bittnar Z and Gerard B, Eds), Hermes Science Publications, pp. 55–77

[13] Willam K J and Warnke E P 1975 *Constitutive model for the triaxial behaviour of concrete, IABSE Seminar on concrete structures subjected to triaxial stress*, Bergamo, Italy, pp. 1–31

[14] Pietruszczak S, Jiang J and Mirza F A 1988 *An elastoplastic constitutive model for concrete, Int. J. Solid Struct.* **24** (7) 705

[15] Menetrey P and Willam K J 1995 *Triaxial failure criterion for concrete and its generalization, ACI Struct. J.* **92** 311

[16] Bobiński J and Tejchman J 2004 *Numerical simulations of localization of deformation in quasi-brittle materials within non-local softening plasticity, Comp. Concr.* **4** 433

[17] Dragon A and Mroz Z 1979 *A continuum model for plastic-brittle behaviour of rock and concrete, Int. J. Eng. Sci.* **17** 121

[18] Peerlings R H J, de Borst R, Brekelmans W A M and Geers M G D 1998 *Gradient enhanced damage modelling of concrete fracture, Mech. Coh.-Frict. Mater.* **3** 323

[19] Chen E 1999 *Non-local effects on dynamic damage accumulation in brittle solids, Int. J. Num. Anal. Meth. Geomech.* **23** 1

[20] Bobiński J and Tejchman J 2005 *Modelling of concrete behaviour with a non-local continuum damage approach, Arch. Hydro-Eng. Env. Mech.* **52** (3) 243

[21] Lemaitre J 1985 *Coupled elasto-plasticity and damage constitutive equations, Comp. Meth. Appl. Mech. Eng.* **51** 31

[22] de Borst R, Pamin J and Geers M G D 1999 *On coupled gradient-dependent plasticity and damage theories with a view to localization analysis, Eur. J. Mech. A/Solids* **18** (6) 939

[23] Ibrahimbegovic A, Markovic D and Gatuing F 2003 *Constitutive model of coupled damage-plasticity and its finite element implementation, Eur. J. Finite Elem.* **12** (4) 381

[24] Salari M R, Saeb S, Willam K J, Patchet S J and Carrasco R C 2004 *A coupled elastoplastic damage model for geomaterials, Comp. Meth. Appl. Mech. Eng.* **193** 2625

[25] Herrmann H J, Hansen A and Roux S 1989 *Fracture of disordered elastic lattices in two dimensions, Phys. Rev. B* **39** 637

[26] Vervuurt A, van Mier J G M and Schlangen E 1994 *Lattice model for analyzing steel-concrete interactions*, *Comp. Meth. Adv.Geomech.* (Siriwardane and Zaman, Eds), Balkema, Rotterdam, pp. 713–718

[27] Schlangen E and Garboczi 1997 *Fracture simulations of concrete using lattice models: computational aspects*, *Eng. Fracture Mech.* **57** 319

[28] Kozicki J and Tejchman J 2006 *2D lattice model for fracture in brittle materials*, *Arch. Hydro-Eng. Env. Mech.*, Polish Academy of Sciences (under press)

[29] Cusatis G, Bazant Z and Cedolin I 2003 *Confinement shear lattice model for concrete damage in tension and compression*, *J. Eng. Mech. ASCE* **129** (12) 1439

[30] Sakaguchi H and Mühlhaus H-B 1997 *Mesh free modelling of failure and localisation in brittle materials* (Asaoka A, Adachi T and Oka F, Eds), *Deformation and Progressive Failure in Geomechanics*, Pergamon, pp. 15–21

[31] D'Addetta G A, Kun F and Ramm E 2002 *In the application of a discrete model to the fracture process of cohesive granular materials*, *Granular Matter* **4** 77

[32] Donze F V, Magnier S A, Daudeville L, Mariotti C and Davenne L 1999 *Numerical study of compressive behaviour of concrete at high strain rates*, *J. Eng. Mech.* **125** 1154

[33] de Borst R, Mühlhaus H-B, Pamin J and Sluys L 1992 *Computational modelling of localization of deformation* (Owen D R J, Onate H and Hinton E, Eds), *Proc. of the 3rd Int. Conf. Comp. Plasticity*, Swansea, Pineridge Press, pp. 483–508

[34] Pamin J and de Borst R 1998 *Simulation of crack spacing using a reinforced concrete model with an internal length parameter*, *Arch. Appl. Mech.* **68** (9) 613

[35] Akkermann J 2000 *Rotationsverhalten von Stahlbeton-Rahmenecken. Dissertation*, Universitat Fridericiana zu Karlsruhe, Karlsruhe

[36] Pijaudier-Cabot G and Bazant Z P 1987 *Nonlocal damage theory*, *ASCE J. Eng. Mech.* **113** 1512

[37] Sluys L J 1992 *Wave propagation, localisation and dispersion in softening solids*, PhD Thesis, Delft University of Technology

[38] Sluys L J and de Borst R 1994 *Dispersive properties of gradient and rate-dependent media*, *Mech. Mater.* **183** 131

[39] *Abaqus Theory Manual. Version 5.8*, Hibbit, Karlsson & Sorensen Inc. 1998

[40] Lemaitre J and Chaboche J L 1990 *Mechanics of Solid Materials*, Cambridge University Press, Cambridge, UK

[41] Bobiński J and Tejchman J 2006 *Modelling of size effects in concrete using elasto-plasticity with non-local softening*, *Arch. Civ. Eng.* LII **1** 7

[42] Kaczanov L M 1986 *Introduction to Continuum Damage Mechanics*, Martimus Nijhoff, Dordrecht

[43] Simo J C and Ju J W 1987 *Strain- and stress-based continuum damage models – I. Formulation*, *Int. J. Solid Struct.* **23** (7) 821

[44] Jirasek M and Marfia S 2005 *Non-local damage model based on displacement averaging*, *Int. J. Num. Meth. Eng.* **63** 77

[45] Simone A and Sluys L 2004 *Continous-discontinous modeling of mode-I and mode-II failure. Modelling of Cohesive-Frictional Materials* (Vermeer P A, Ehlers W, Herrmann H J and Ramm E, Eds), Balkema, pp. 323–337

[46] Bazant Z P and Jirasek M 2002 *Nonlocal integral formulations of plasticity and damage: survey of progress*, *J. Eng. Mech.* **128** (11) 1119

[47] Bazant Z P and Lin F B 1987 *Non-local yield limit degradation*, *J. Eng. Mech. ASCE* **113** 1512

[48] Brinkgreve R B J 1994 *Geomaterial models and numerical analysis of softening*, PhD Thesis, Delft University of Technology

[49] Bazant Z P and Oh B H 1983 *Crack band theory for fracture of concrete*, *Mater. Struct.*, *RILEM* **16** 155

[50] Geers M, Peijs T, Brekelmans W and de Borst R 1996 *Experimental monitoring of strain localization and failure behaviour of composite materials*, *Compos. Sci. Technol.* **56** 1283

[51] Mahnken R and Kuhl E 1999 *Parameter identification of gradient enhanced damage models*, *Eur. J. Mech. A/Solids* **18** 819

[52] Le Bellego C, Dube J F, Pijaudier-Cabot G and Gerard B 2003 *Calibration of nonlocal damage model from size effect tests*, *Eur. J. Mech. A/Solids* **22** 33

[53] Pijaudier-Cabot G, Haidar K and Dube J F 2004 *Non-local damage model with evolving internal length*, *Int. J. Num. Anal. Meths. Geomech.* **28** 633

[54] Ferrara I and di Prisco M 2001 *Mode I fracture behaviour in concrete: nonlocal damage modeling*, *ASCE J. Eng. Mech.* **127** (7) 678

[55] Bhandari A R and Inoue J 2005 *Experimental study of strain rates effects on strain localization characteristics of soft rocks*, *Soils and Foundations* **45** (1) 125

[56] Bobiński J and Tejchman J 2006 *Modelling of strain localization in quasi-brittle materials with non-local continuum models*, *Comp. Model. Concr. Struct.*, *EURO-C* (Meschke G, de Borst R, Mang H and Bicanic N, Eds), Taylor and Francis, pp. 301–307

[57] Grassl P and Jirasek M 2006 *Plastic model with non-local damage applied to concrete*, *Int. J. Num. Anal. Meth. Geomech.* **30** 71

[58] Ortiz M and Simo I C 1986 *An analysis of a new class of integration algorithms foe elastoplastic constitutive relation*, *Int. J. Num. Meth. Eng.* **23** 353

[59] Hughes T J R and Winget J 1980 *Finite rotation effects in numerical integration of rate constitutive equations arising in large deformation analysis*, *Int. J. Num. Meth. Eng.* **15** 1862

[60] Hordijk D A 1991 *Local approach to fatigue of concrete*, PhD Thesis, Delft University of Technology

[61] Jirasek M and Rolshoven S 2003 *Comparison of integral-type nonlocal plasticity models for strain-softening materials*, *Int. J. Eng. Sci.* **41** 1553

[62] Małecki T, Marzec I, Bobiński J and Tejchman J 2006 *FE-analysis of crack spacing in a reinforced concrete bar under tension using elasto-plasticity with non-local softening*, *Arch. Civ. Eng.* (submitted)

[63] Gutierrez M A and de Borst R 2003 *Simulation of size-effect behaviour through sensitivity analysis*, *Eng. Fracture Mech.* **70** 2269

[64] Pamin J 2004 *Gradient-enchanced continuum models: formulation, discretization and applications. Habilitation Monography*, Cracow University of Technology, Cracow

[65] Rodriguez-Ferran A, Morata I and Huerta A 2002 *Numerical modelling of notched specimens*, *Proc. WCCM V*, Vienna, Austria (CD edition)

[66] Pamin J 2005 *Gradient plasticity and damage models: a short comparison*, *Comp. Mater. Sci.* **32** 472

[67] Zhou W, Zhao J, Liu Y and Yang Q 2002 *Simulation of localization failure with strain-gradient-enhanced damage mechanics*, *Int. J. Num. Anal. Meth. Geomech.* **26** 793

[68] Walukiewicz H, Bielewicz E and Gorski J 1997 *Simulation of nonhomegeneous random fields for structural applications*, *Comp. Struct.* **64** (1–4) 491

[69] Tejchman J 2006 *Effect of fluctuation of current void ratio on the shear zone formation in granular bodies within micro-polar hypoplasticity*, *Comp. Geotech.* (under press)

[70] Kozicki J and Tejchman J 2006 *Measurements of the displacement field in concrete notched beams using a digital image correlation (DIC) technique*, *Lect., Int. Conf. EURO-C*, Mayrhofen